# Supporting Information

## A Dicyanobenzoquinone Based Cathode Material for Rechargeable Lithium and Sodium Ion Batteries**

*Hailong Lyu, Charl J. Jafta, Ilja Popovs, Harry M. Meyer III,[b] Jordan A. Hachtel,[c] Jingsong Huang,* Bobby G. Sumpter, Sheng Dai, and Xiao-Guang Sun**

To calculate the capacity contributions of the redox reactions of DCBQ, the Faradaic reactions of the surface oxygen functional groups, and the super capacitance adsorption on the large surface of the CNTs towards the total capacity of CNTs-DCBQ, CVs of the CNTs, CNTs-COOH and CNTs-DCBQ in the restricted voltage range of 2.0-3.8 V in **Figure 2a** were used. The capacity contribution of the redox reactions of DCBQ was calculated by subtracting the integral area of the CNTs-COOH CV from that of the CNTs-DCBQ CV, whereas the capacity contributions of the oxygen functional groups and that of the super capacitance adsorption on the large surface areas of CNTs was evaluated by subtracting the integral area of the CNTs CV curve from that of the CNTs-COOH CV curve and by the integral area of the CNTs CV curve, respectively. The result shows that 28.2 %, 55.4 % and 16.4 % of the CNTs-DCBQ CV is from the redox reactions of DCBQ, the Faradaic reactions of the surface oxygen functional groups and the super capacitance adsorption on the large surface of the CNTs, corresponding to 47.9, 94.2 and 27.9 mAh $g^{-1}$, respectively. According to 14.62 wt.% of DCBQ in CNTs-DCBQ, the specific capacity based on DCBQ content is calculated to be 328 mAh $g^{-1}$, which is close to theoretical capacity of DCBQ (339 mAh $g^{-1}$).

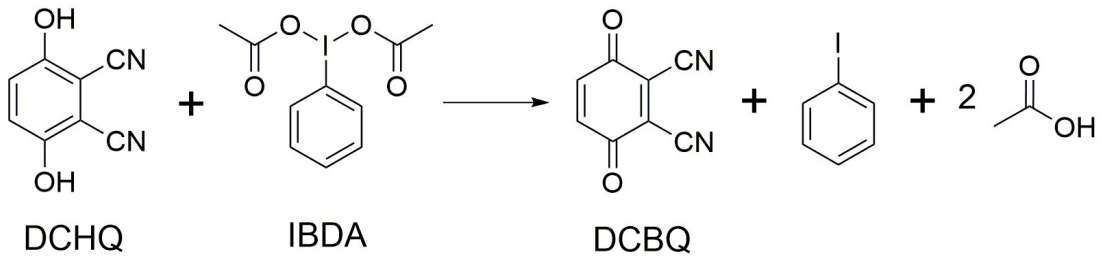


**Scheme S1**. Oxidation of 2,3-dicyanohydroquinone (DCHQ) with iodobenzene diacetate (IBDA)

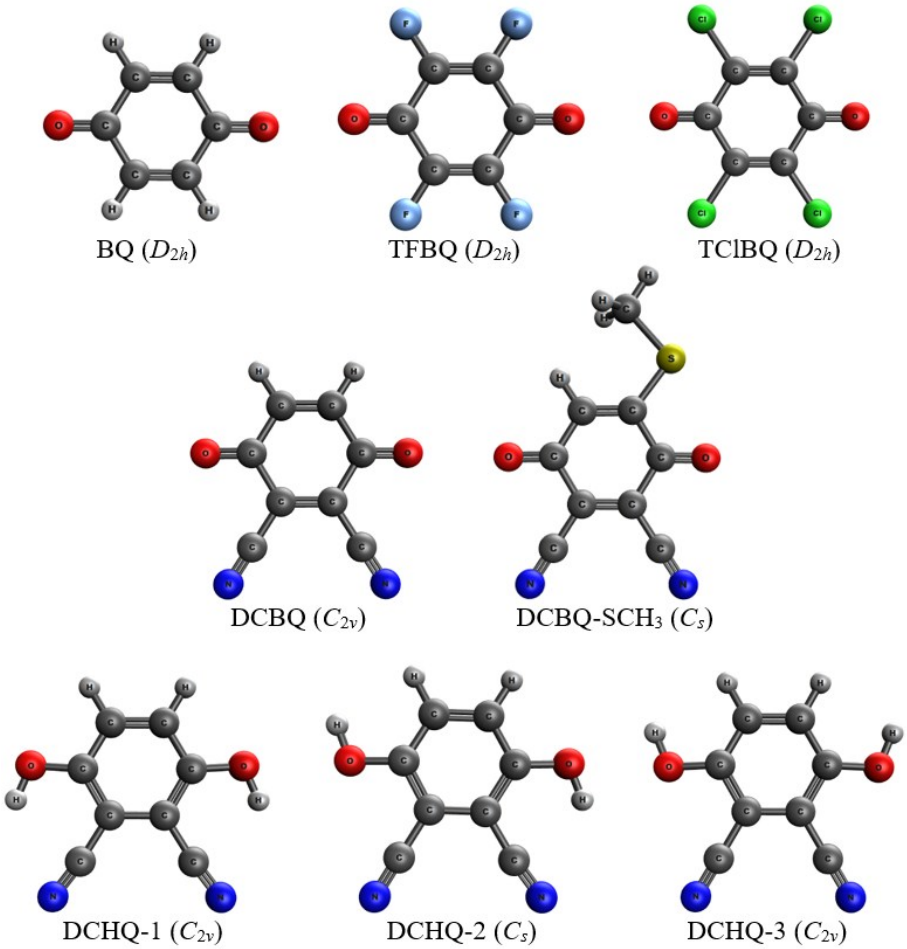


**Figure S1.** Structures and point group symmetry labels in parentheses for BQ, TFBQ, TClBQ, DCBQ, DCBQ-SCH$_3$, DCHQ-1, DCHQ-2, and DCHQ-3 tabulated in Tables S1 and S2.

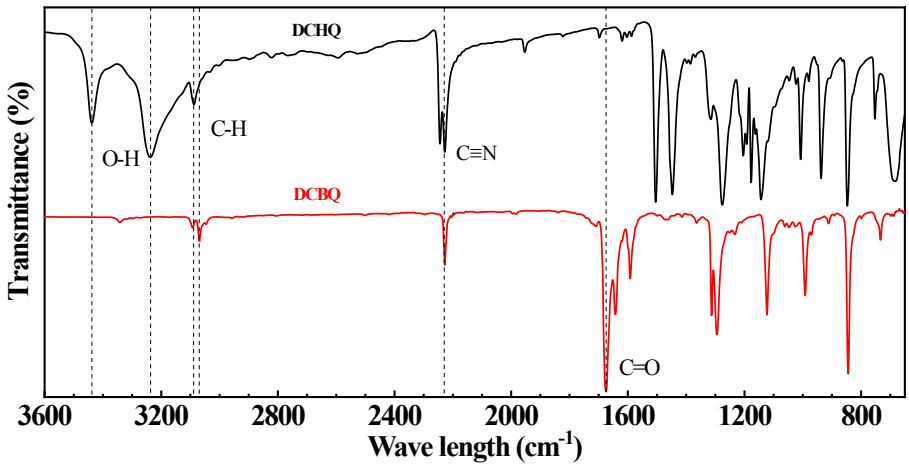


**Figure S2.** FTIR spectra of DCHQ and DCBQ. Vertical dashed lines are used to indicate the vibrational frequencies of the key functional groups such as O-H, C-H, C≡N, and C=O.

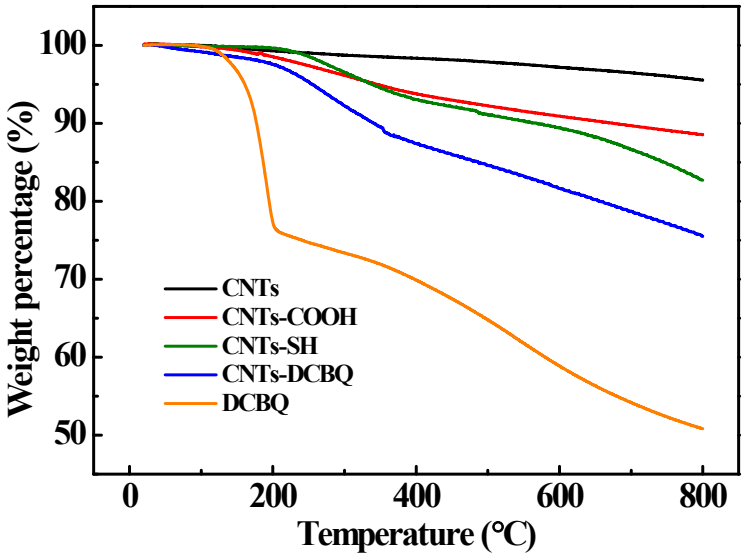


**Figure S3.** TGA curves of CNTs, CNTs-COOH, CNTs-SH, CNTs-DCBQ and DCBQ in $N_2$ with a heating rate of 10 °C $min^{-1}$.

TGA measurement was used to monitor the functionalization of CNTs at each step. **Figure S3** shows the TGA plots of pristine CNTs, CNTs-COOH, CNTs-SH, CNTs-DCBQ and pure DCBQ. The weight loss of CNTs-COOH is 11.47% after heating up to 800 °C, which is more than double that of the pristine CNTs under the same test conditions (4.45%). The increased weight loss can be attributed to the loss of functional groups introduced onto the CNTs surface. For CNTs-SH and CNTs-DCBQ, the weight loss is 17.28% and 24.47%, respectively. The gradual increase in weight loss is ascribed to the decomposition of the mercapto groups and the bounded DCBQs. According to the total 49.17% weight loss of pure DCBQ and the 7.19% difference in weight loss between CNTs-SH and CNTs-DCBQ, the content of grafted DCBQ on the oxidized CNTs is estimated to be 14.62 wt%.

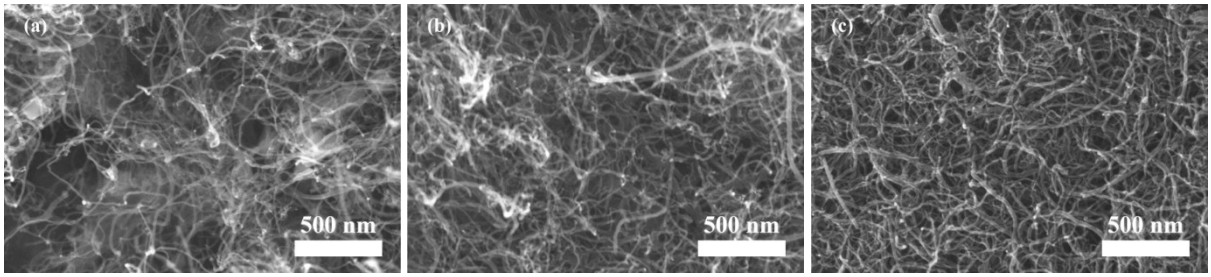


**Figure S4.** SEM images of a) CNTs, b) CNTs-COOH, and c) CNTs-SH.

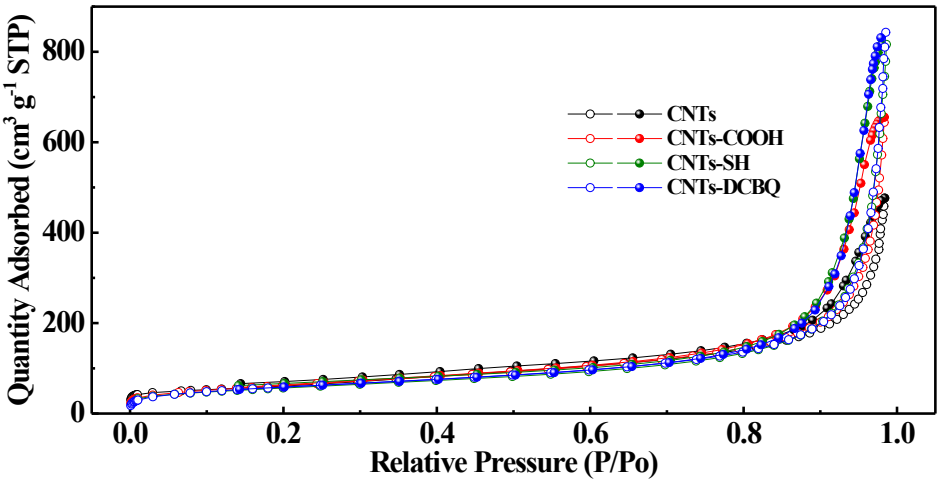


**Figure S5.** $N_2$ adsorption-desorption isotherms of CNTs, CNTs-COOH, CNTs-SH and CNTs-DCBQ.

**Figure S5** shows that the multiple step functionalization of CNTs-DCBQ does not affect the specific surface area of the CNTs, that is, 218.3, 226.8, 204.7, and 215.3 $m^2 g^{-1}$ for CNTs, CNTs-COOH, CNTs-SH and CNTs-DCBQ, respectively.

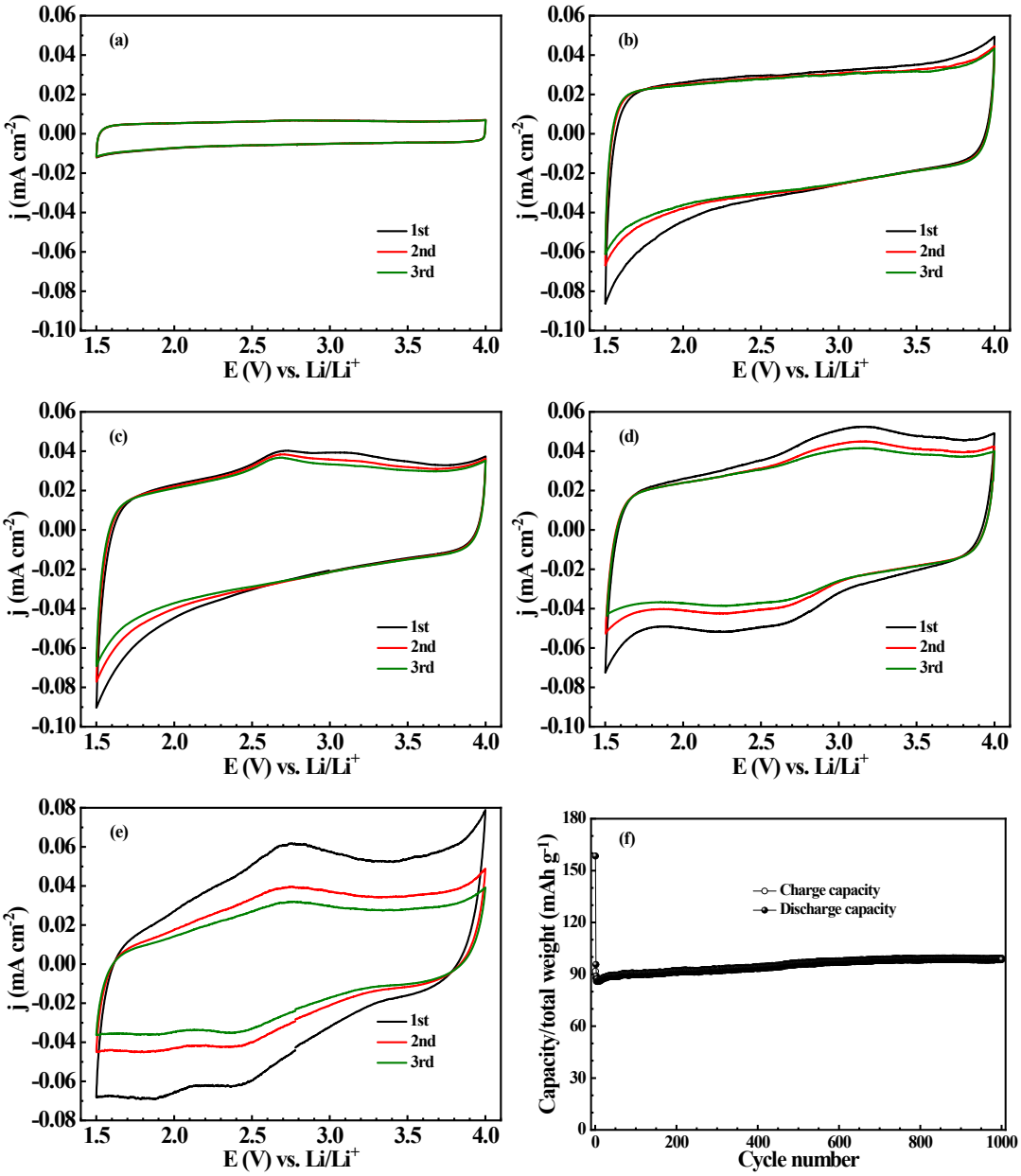


**Figure S6.** Cyclic voltammograms (CVs) of a) CNTs, b) CNTs-COOH, c) CNTs-SH, d) CNTs-DCBQ and e) CNTs-BQ LIB half-cells for the initial three cycles at a scan rate of 0.5 mV $s^{-1}$. f) Charge-discharge capacities of the CNTs-BQ based LIB half-cell at a current density of 200 mA $g^{-1}$.

**Figure S6** shows the first three cycles of the CVs for LIB cells of CNTs, CNTs-COOH, CNTs-SH, CNTs-DCBQ and CNTs-BQ, as well as the charge-discharge capacities of the LIB half-cell based on CNTs-BQ at a current density of 200 mA $g^{-1}$. Except for CNTs, the CV loop areas of the other four cells gradually decrease with cycling, consistent with the initial capacity fading discussed below. It is noted that, the CV curve area of CNTs-BQ reduce drastically after the first cycle, corresponding to the large capacity loss for the initial cycle shown in **Figure S6f**, which can be ascribed to the irreversible reactions of BQ during the first discharge. Besides, the redox-peak of CNTs-BQ is about 0.5 V lower than that of CNTs-DCBQ due to the electron withdrawing effect of the cyano groups in the latter, consistent with the results of the CVs of monomers shown in **Figure S7**.

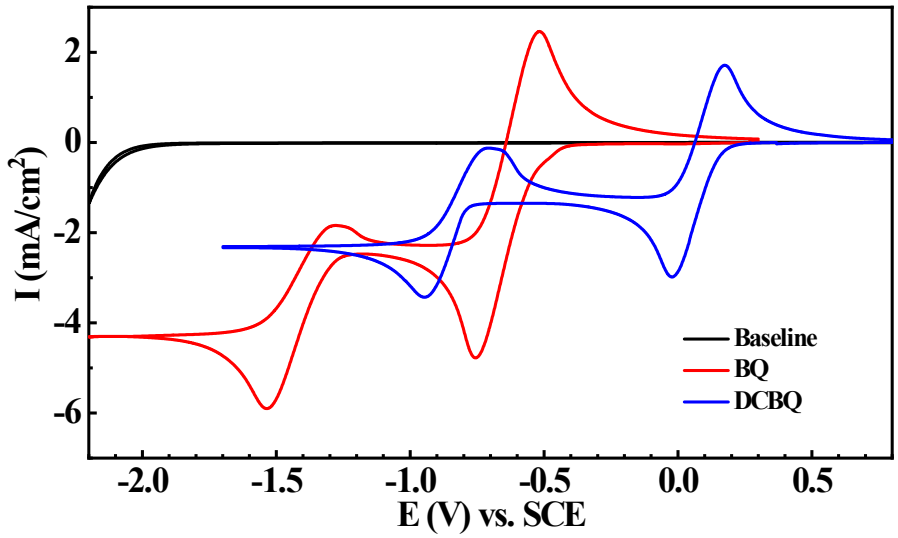


**Figure S7**. Cyclic voltammograms (CVs) of BQ and DCBQ at a scan rate of 20 mV/s.

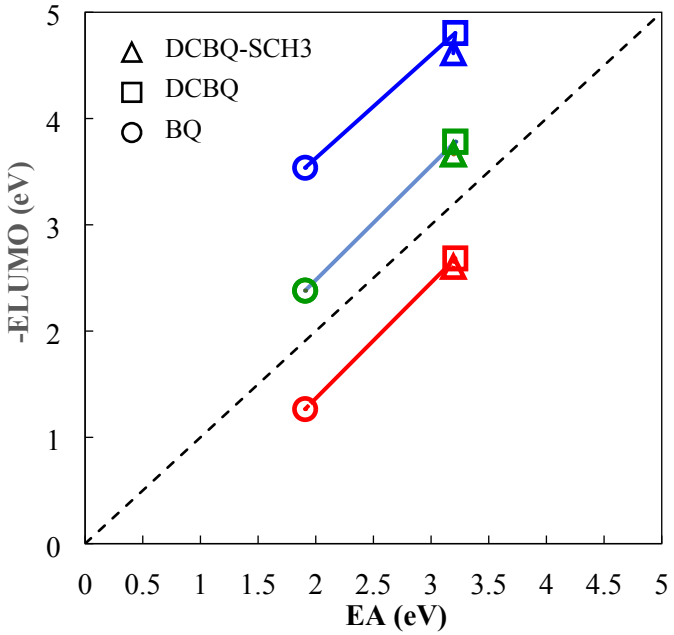


**Figure S8.** Correlation between electron affinities (EAs) calculated by G3MP2B3 (**Table S1**) and -$E_{LUMO}$ for BQ, DCBQ, and DCBQ-$SCH_3$ calculated by three representative exchange-correlation functionals B3LYP (blue), BHandHLYP (green), and LC-wPBE (red).

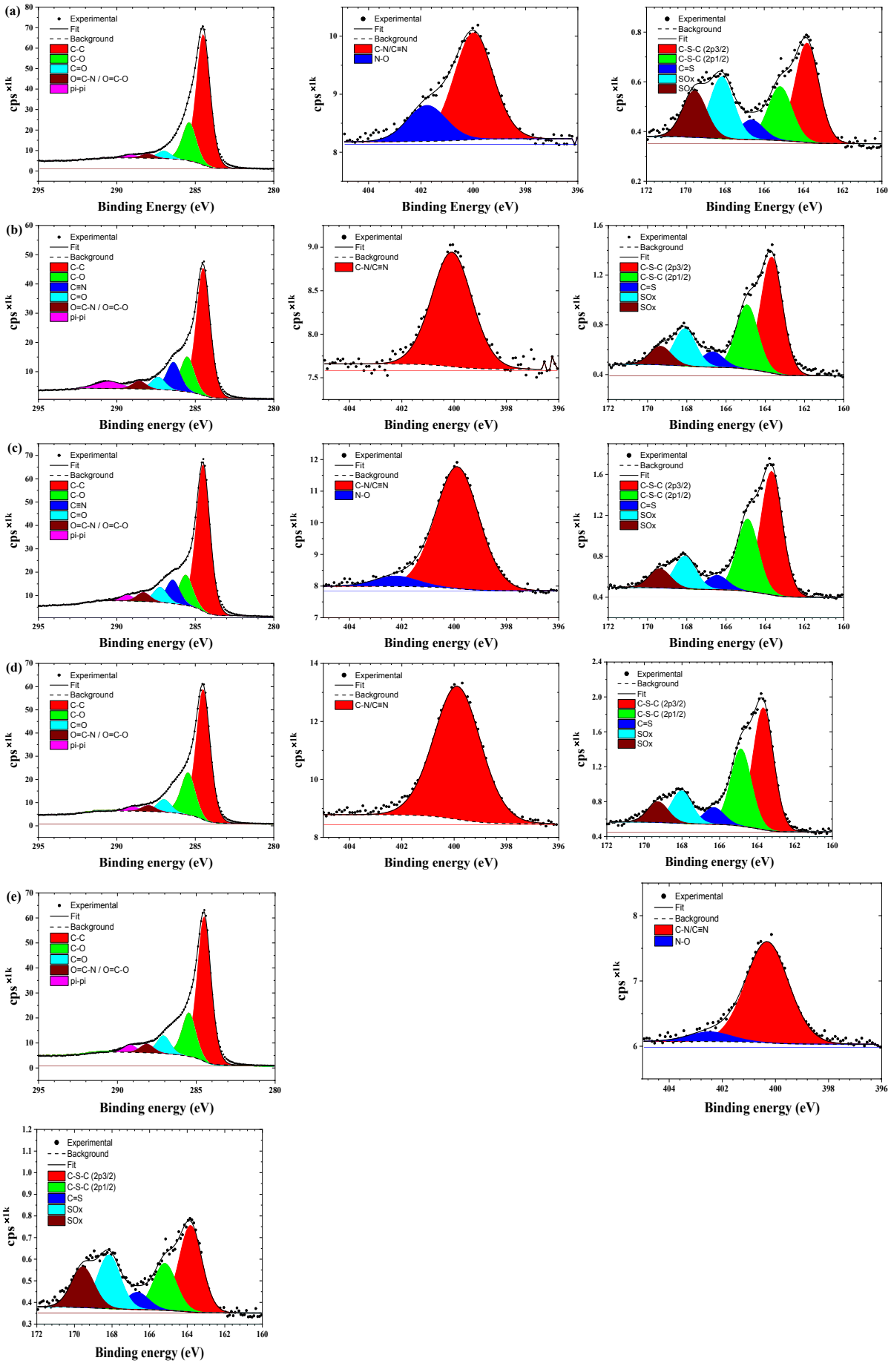
(a)
Experimental
Fit
Background
C-C
C-O
C=O
O=C-N / O=C-O
pi-pi
cps ×1k
Binding Energy (eV)
Experimental
Fit
Background
C-N/C≡N
N-O
cps ×1k
Binding Energy (eV)
Experimental
Background
Fit
C-S-C (2p3/2)
C-S-C (2p1/2)
C=S
SOx
SOx
cps ×1k
Binding Energy (eV)
(b)
Experimental
Fit
Background
C-C
C-O
C≡N
C=O
O=C-N / O=C-O
pi-pi
cps ×1k
Binding energy (eV)
Experimental
Fit
Background
C-N/C≡N
cps ×1k
Binding energy (eV)
Experimental
Background
Fit
C-S-C (2p3/2)
C-S-C (2p1/2)
C=S
SOx
SOx
cps ×1k
Binding energy (eV)
(c)
Experimental
Fit
Background
C-C
C-O
C≡N
C=O
O=C-N / O=C-O
pi-pi
cps ×1k
Binding energy (eV)
Experimental
Fit
Background
C-N/C≡N
N-O
cps ×1k
Binding energy (eV)
Experimental
Background
Fit
C-S-C (2p3/2)
C-S-C (2p1/2)
C=S
SOx
SOx
cps ×1k
Binding energy (eV)
(d)
Experimental
Fit
Background
C-C
C-O
C=O
O=C-N / O=C-O
pi-pi
cps ×1k
Binding energy (eV)
Experimental
Fit
Background
C-N/C≡N
cps ×1k
Binding energy (eV)
Experimental
Background
Fit
C-S-C (2p3/2)
C-S-C (2p1/2)
C=S
SOx
SOx
cps ×1k
Binding energy (eV)
(e)
Experimental
Fit
Background
C-C
C-O
C=O
O=C-N / O=C-O
pi-pi
cps ×1k
Binding energy (eV)
Experimental
Fit
Background
C-N/C≡N
N-O
cps ×1k
Binding energy (eV)
Experimental
Background
Fit
C-S-C (2p3/2)
C-S-C (2p1/2)
C=S
SOx
SOx
cps ×1k
Binding energy (eV)

Figure S9. X-ray photoelectron spectra (XPS) of C1s (left), N1s (center) and S2p (right) for a) CNTs-SH, b) CNTs-DCBQ, c) cycled CNTs-DCBQ, d) CNTs-BQ, and e) cycled CNTs-BQ.

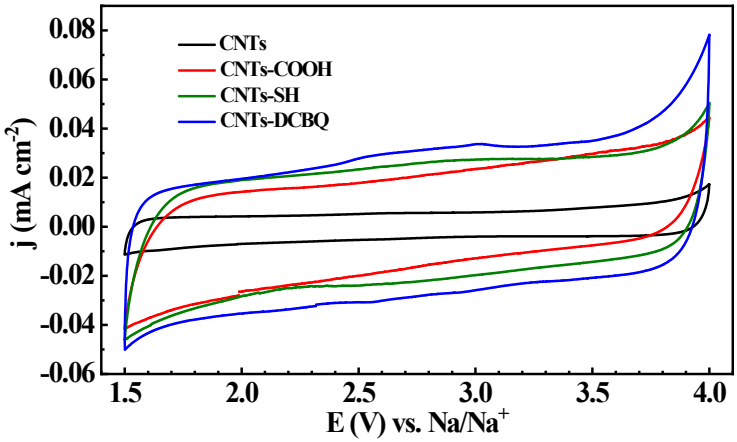


**Figure S10.** Cyclic voltammograms (CVs) of CNTs, CNTs-COOH, CNTs-SH and CNTs-DCBQ SIB half-cells at a scan rate of 0.5 mV $s^{-1}$.

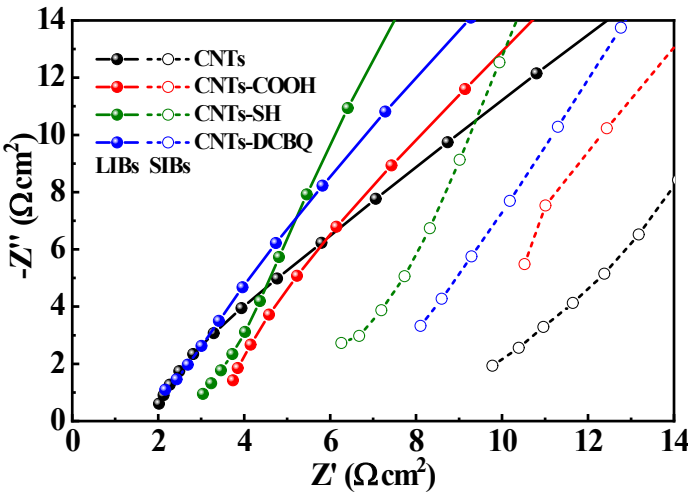


**Figure S11.** High-frequency intersection of the EIS for the LIB and SIB half-cells of CNTs, CNTs-COOH, CNTs-SH and CNTs-DCBQ before cycling.

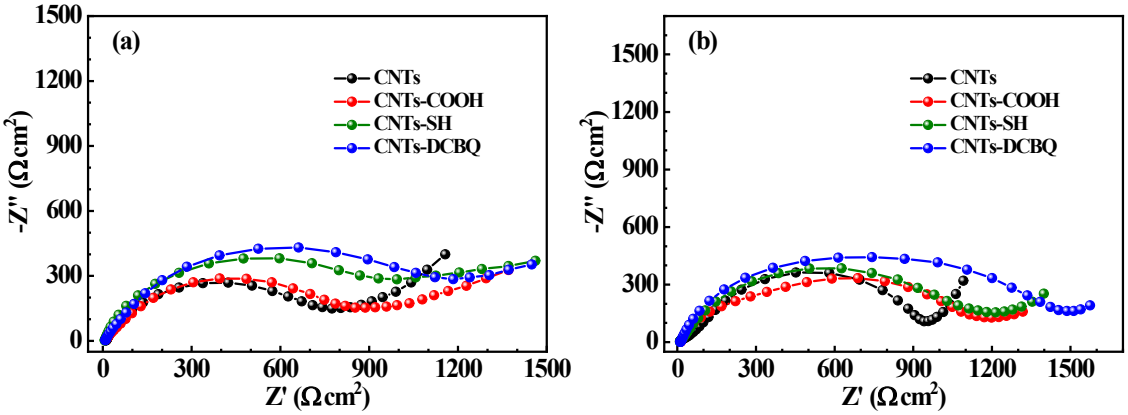


**Figure S12.** Electrochemical impedance spectra (EIS) of the SIB half-cells based on CNTs, CNTs-COOH, CNTs-SH and CNTs-DCBQ a) before cycling and b) after 1000 cycles at 200 mA $g^{-1}$.

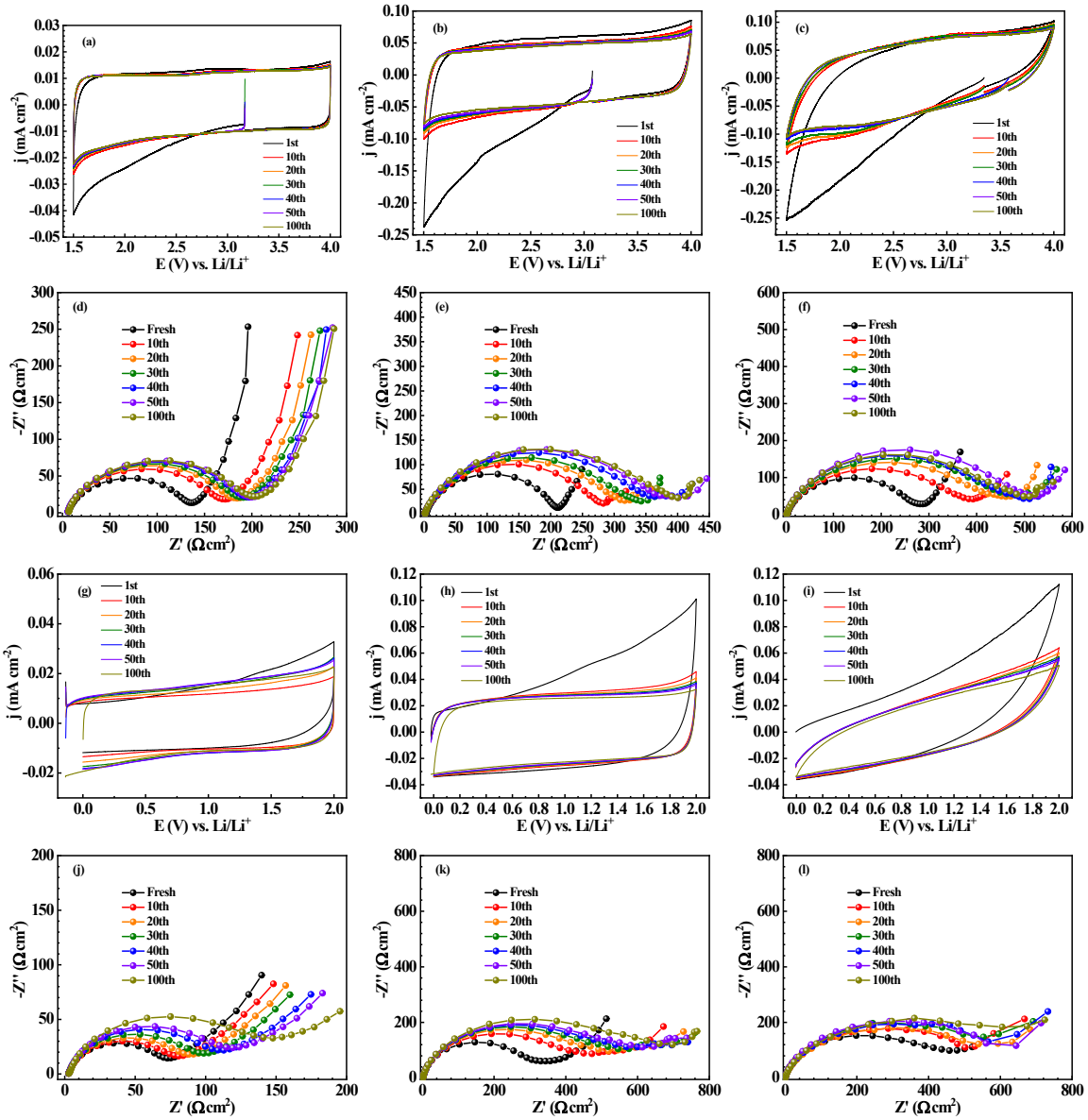


**Figure S13.** Cyclic voltammograms (CVs) of CNTs (left), CNTs-COOH (center), and CNTs-DCBQ (right) LIB half-cells (a-c) and symmetric cells (g-i) for the selected cycles at a scan rate of 2 mV $s^{-1}$. Electrochemical impedance spectra (EIS) of the LIB half-cells (d-f) and symmetric cathode cells (j-l) based on CNTs (left), CNTs-COOH (center), and CNTs-DCBQ (right) after different CV cycles.

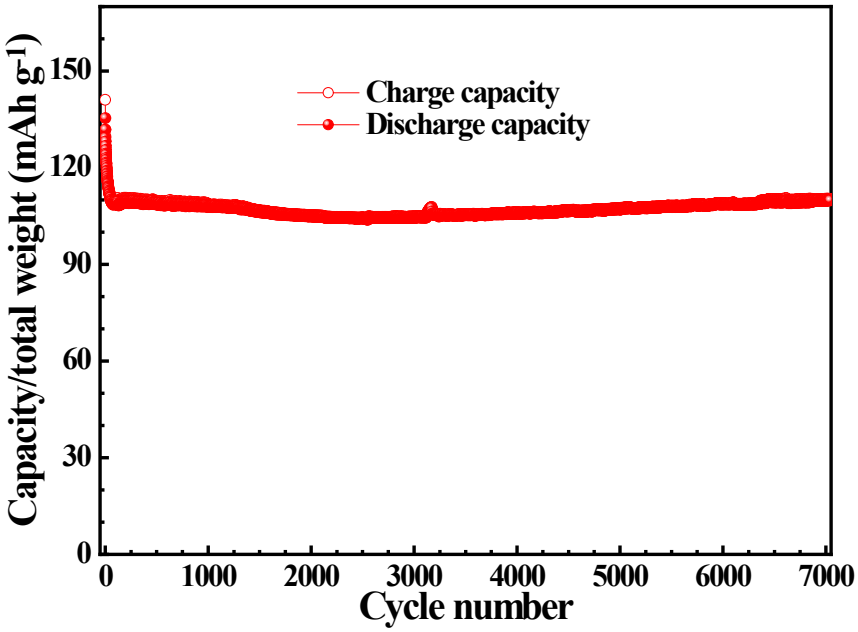


**Figure S14.** Long cycling performance of the CNTs-DCBQ based LIB half-cell at a current rate of 200 mA $g^{-1}$.

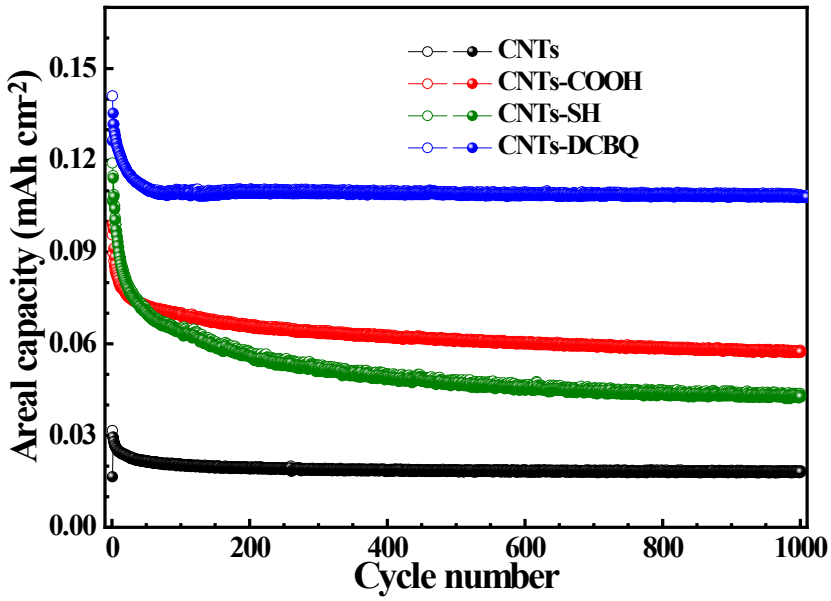


**Figure S15.** Areal capacities of the LIB half-cells based on CNTs, CNTs-COOH, CNTs-SH and CNTs-DCBQ at a current density of 200 mA $g^{-1}$. (Hollow circles – and solid spheres □ represent charge and discharge capacities, respectively).

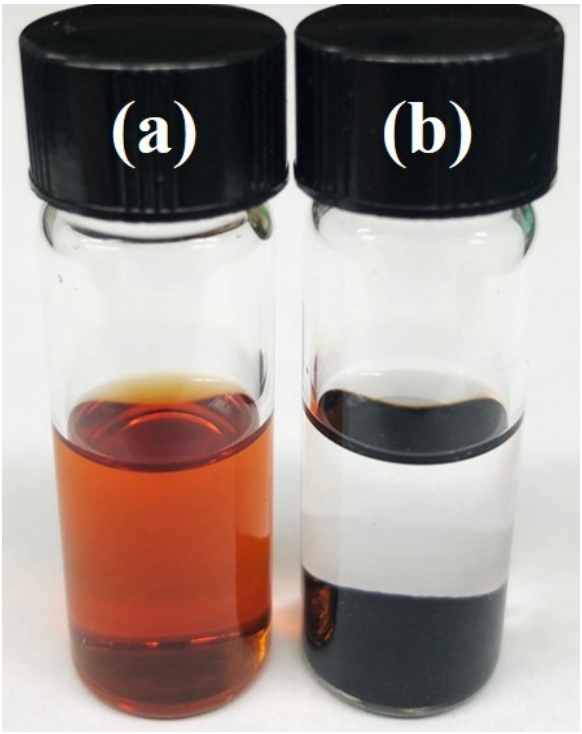


**Figure S16.** Digital photos of a) 20 mg DCBQ and b) 50 mg CNTs-DCBQ in 5 ml 1 M $LiPF_6$/EC-DEC-DMC (1:1:1, vol.) for one week.

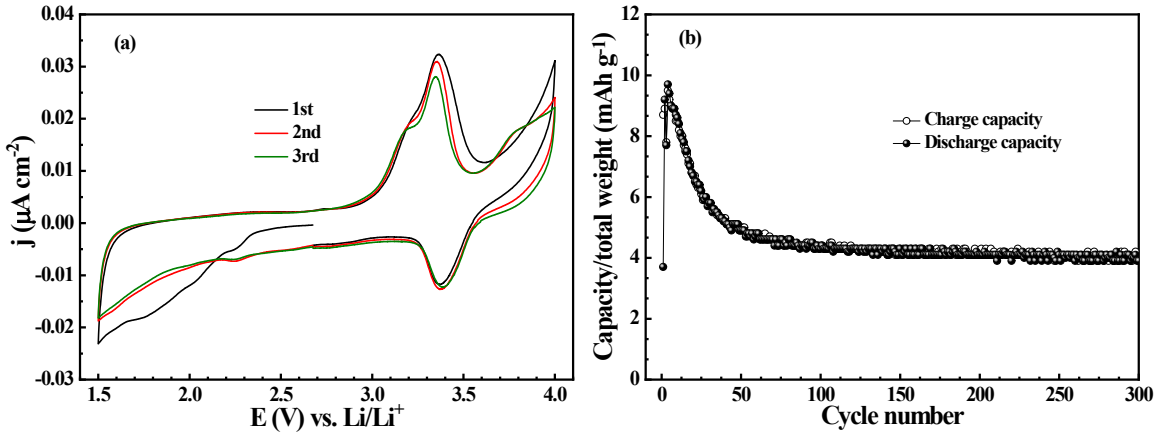


**Figure S17.** a) CVs of DCBQ LIB half-cells for the initial three cycles at a scan rate of 0.5 mV $s^{-1}$. b) Charge-discharge capacities of the DCBQ based LIB half-cell at a current density of 200 mA $g^{-1}$.

**Table S1.** Electron affinities (EA) in eV calculated by G3MP2B3 composite method for BQ, TFBQ, TClBQ, DCBQ, and DCBQ-$SCH_3$.

| Species | Charge q | G° (Eh) | EA (eV) |
|---|---|---|---|
| BQ[a] | 0 | -380.953022 | 1.908, 1.91±0.10[b] |
| | -1 | -381.023138 | |
| TFBQ[a] | 0 | -777.582040 | 2.691, 2.70±0.10[b] |
| | -1 | -777.680923 | |

| | | | |
|---|---|---|---|
| TClBQ[a] | 0 | -2217.605077 | 2.788, 2.78±0.10[b] |
| | -1 | -2217.707527 | |
| DCBQ[c] | 0 | -565.209556 | 3.210 |
| | -1 | -565.327524 | |
| DCBQ-$SCH_3$[d,e] | 0 | -1002.216908 | 3.193 |
| | -1 | -1002.334265 | |

[a] Experimental EAs of BQ, TFBQ, and TClBQ are used to validate the G3MP2B3 method. [b] Experimental results from the literature.[1] [c] Theoretical EA of DCBQ shows the strong electron-withdrawing effects of cyano groups. [d] DCBQ-$SCH_3$ is relevant because DCBQs were anchored on CNT scaffolds through the thioether bonds; its theoretical EA shows that the methylsulfanyl -$SCH_3$ group may slightly lower the electron affinity of DCBQ due to its electron donating effects. [e] Results for the global minimum only; calculations were also done for local minimum but not shown.

**Table S2.** Vibrational frequencies from B3LYP/6-31G* calculations, using the recommended scaling factor of 0.96 for the used model chemistry, in comparison with values from the experimental FTIR spectra.

| Species[a] | $E_{rel}$[b] | O-H ($cm^{-1}$)[c,d] | C-H ($cm^{-1}$)[c,d] | C≡N ($cm^{-1}$)[c,d] | C=O ($cm^{-1}$)[c,d] |
|---|---|---|---|---|---|
| DCHQ-1 | 0 | 3542 (s), 3541 (a) | 3105 (s, w), 3094 (a, w) | 2241 (a), 2238 (s) | -- |
| DCHQ-2 | 3.02 | 3606, 3538 | 3101(w), 3060 | 2258, 2241 | -- |
| DCHQ-3 | 6.39 | 3607 (s), 3606 (a) | 3068 (s), 3054 (a) | 2262 (a), 2259 (s) | -- |
| DCBQ | -- | -- | 3101 (s, w), 3087 (a, w) | 2263 (a), 2254 (s) | 1698 (a), 1692 (s, w) |
| DCHQ (exp) | -- | 3436, 3238 | 3087 | 2243, 2228 | -- |
| DCBQ (exp) | -- | -- | 3087, 3069 | 2228 | 1686 |

[a] DCHQ-1, DCHQ-2, and DCHQ-3 correspond to the global minimum and two local minima of DCHQ (Figure S1). [b] Relative energies $E_{rel}$ in kcal/mol were calculated by the total energies of local minima relative to the global minimum. [c] The agreements between theoretical and experimental results are good for all vibrational modes except for O-H vibrations due to the fact that the theoretical calculations were performed for isolated molecules but in experimental FTIR measurements there exist intermolecular hydrogen bonds in the condensed phase. [d] Labels (s) and (a) refer to symmetric and asymmetric stretching modes and (w) represents weak peaks.

**Table S3.** Elemental analysis of CNTs-DCBQ

| **Element** | C | H | N | S |
|---|---|---|---|---|
| **Content (%)** | 83.16 | 0.99 | 3.72 | 3.31 |

**Table S4.** Electrochemical properties of Quinone/CNTs composite electrodes

| Quinone/ CNTs composites | Quinone content | Capacity (mAh $g^{-1}$) by quinone weight /total weight | Current density (mA $g^{-1}$) | Capacity Retention (Cycles) |
|---|---|---|---|---|
| AQ@ SWCNTs for LIB [2] | 25 wt% 9,10-anthraquinone (AQ) | 260/65 | 100/ Quinone wt. | 35% (50) |
| PhQ@ SWCNTs for LIB [2] | 18 wt% 9,10-phenanthrenequinone (PhQ) | 280 /50 | 100/ Quinone wt. | 45% (50) |
| PhQ@ SWCNT-1.5 for LIB [3] | 22 wt% 9,10-phenanthrenequinone (PhQ) | 180/40 | 100/ Quinone wt. | N/A |
| PhQ@ SWCNT-1.5 for SIB [3] | 22 wt% 9,10-phenanthrenequinone (PhQ) | 200/44 | 100/ quinone wt. | N/A |
| Emodin/ SCNT for LIB [4] | 59.6 wt% Emodin | 270/161 | 100/ quinone wt. | 44% (50) |
| P($4VC_{86}$-*stat*-$LiSS_{14}$)/ CNT for LIB [5] | 22 wt% P($4VC_{86}$-*stat*-$LiSS_{14}$) | 315/63 | 450/total wt. | 98% (3400) |
| PBDTD@ CNT for LIB [6] | 80.9 wt% cross-conjugated quinone oligomer (PBDTD) | 175/85 | 1071/ quinone wt. | 96% (250) |
| CNTs-DCBQ for LIB (this work) | 14.6 wt% (DCBQ) | 754.8/110.2 | 200/total wt. | 100% (7000) |
| CNTs-DCBQ for SIB (this work) | 14.6 wt% (DCBQ) | 598.6/87.4 | 200/total wt. | 94% (1000) |

**References:**


[1] T. Heinis, S. Chowdhury, S. L. Scott, P. Kebarle, *J. Am. Chem. Soc.* **1988**, 110, 400.
[2] Y. Ishii, K. Tashiro, K. Hosoe, A. Al-zubaidi, S. Kawasaki, *PCCP* **2016**, 18, 10411.
[3] L. Canghao, I. Yosuke, I. Shunya, K. Shinji, *Nanotechnology* **2017**, 28, 355401.
[4] P. Hu, H. Wang, Y. Yang, J. Yang, J. Lin, L. Guo, *Adv. Mater.* **2016**, 28, 3486.
[5] N. Patil, A. Aqil, F. Ouhib, S. Admassie, O. Inganäs, C. Jérôme, C. Detrembleur, *Adv. Mater.* **2017**, 29, 1703373.
[6] Y. Jing, Y. Liang, S. Gheytani, Y. Yao, *Nano Energy* **2017**, 37, 46.